Visible-light assisted surface plasmon resonance triggered Ag/ZnO nanocomposites: synthesis and performance towards degradation of indigo carmine dye

Rahul Kumar
Visvesvaraya National Institute of Technology
Shaileshkumar Y. Janbandhu
Visvesvaraya National Institute of Technology
Gaurav K. Sukhadeve
Visvesvaraya National Institute of Technology
Rupesh S. Gedam (rupesh_gedam@rediffmail.com)
Visvesvaraya National Institute of Technology

Research Article

Keywords: Ag/ZnO, Water pollution, Nanocomposites, Visible light, Photocatalysis, Indigo carmine, Dye degradation

Posted Date: May 19th, 2022

DOI: https://doi.org/10.21203/rs.3.rs-1608601/v1

Abstract

Water pollution caused by organic compounds, generated from different industries has gained attention worldwide today. In this regard, significant efforts have been made for suitable dye degradation technology. Zinc oxide (ZnO) based photocatalysts are considered novel materials to degrade organic effluents in contaminated water. The facile synthesis of Ag/ZnO nanocomposites and its application for the enhanced degradation of Indigo carmine (IC) dye under visible light irradiation is reported in this paper. The prepared photocatalysts were characterized using various analytical techniques such as X-ray diffraction (XRD), scanning electron microscopy (SEM), high-resolution transmission electron microscopy (HRTEM), FTIR, Raman, Impedance study, UV-Vis, and photoluminescence (PL). Prepared Ag/ZnO nanocomposites were tested for degradation of IC dye in visible light. The degradation efficiency of IC dye was found to be 95.71% in 120 min, with a rate constant of 0.01957 min^{-1}. This improved photocatalytic activity of Ag/ZnO nanocomposites was mainly due to the absorption of visible light caused by surface plasmon resonance (SPR) derived from Ag nanoparticles (NPs) and electron-hole separation. Radical trapping experiments suggest that holes (h^+), and superoxide radical ($O_2^{\bullet -}$) are the key factors in photocatalytic IC dye degradation.

1. Introduction

With the rising of global population and widespread industrial growth, fossil fuel consumption is rapidly increasing (Guo et al. 2019). As a result, serious environmental pollution (caused by toxic agents and industrial waste) often contains considerable amounts of various organic dye pollutants (Janbandhu et al. 2022). These poured chemicals into the groundwater reservoirs cause irreversible damage to human health and the natural environment. As a consequence, it appears that the elimination of organic dyes from wastewater is extraordinarily important (Lellis et al. 2019). Semiconductor heterogeneous photocatalysis has become a hot topic that sparked interest all around the world, particularly in dye treatment. Over the last decades, various photocatalysts, such as TiO_2 (Sukhadeve et al. 2022), SnO_2 (Elango and Roopan 2016), ZnO (Gao et al. 2013), CdS (Janbandhu et al. 2019a), etc. have been used to degrade water contaminants. Among them, ZnO semiconductor is considered as one of the most promising photocatalyst in the industry as well as for the research community due to its potential applications for the decomposition of many toxic and non-biodegradable organic pollutants. Such catalyst, due to its incredible features like low cost, higher chemical stability, non-toxicity, better sensing behavior, high photocatalytic activity, and so on, makes it a suitable candidate for photocatalysis (Chaudhary et al. 2013; Saravanan et al. 2015). However, ZnO is generally regarded as a non-viable material for practical applications because of its two major limitations. The first particularly limiting factor is a larger bandgap of ZnO (~ 3.37 eV) limits its response to UV light only. The second one is fast recombination of photoexcited charge carriers (Zhang et al. 2017). So, it is important to extend the absorption spectrum of ZnO to include more visible light for boosting photocatalytic efficiency. To overcome these drawbacks, doping with metal or non-metal is considered a useful tool to enhance the photocatalytic activity of ZnO (Georgekutty et al. 2008). Doping a semiconductor entails introducing impurities or other elements to modify its characteristics and improve its photocatalytic activity (Lee et al. 2016).

Most recent numerous studies performed by various researchers that are mainly focused on noble metals such as Pd (Kumari et al. 2020), Pt (Jaramillo-Páez et al. 2018), Au (Bueno-Alejo et al. 2021), and Ag (Zhang et al. 2014), to improve the photocatalytic activity of ZnO (Li et al. 2018). Of these, Ag sensitized ZnO nanomaterials received very much attention because of two reasons: (i) reduction in the recombination rate of photogenerated electron-hole pairs at the metal-semiconductor interface due to the generation of the Schottky barrier. (ii) improvement of visible light absorption performance caused by the surface plasmon resonance (SPR), consequently improves the photocatalytic efficiency (Raji et al. 2018). Compared with other noble metals, silver got more attention due to its high electrical and thermal conductivity, antibacterial characteristics, cost-effectiveness, and non-toxicity (Zhang et al. 2017). Although Ag/ZnO nanocomposites have been widely studied for photocatalytic properties, but there are very few reports on Ag/ZnO nanomaterials for photocatalytic degradation of Indigo Carmine (IC) dye under the illumination of visible light.

This work reports the synthesis of Ag/ZnO nanocomposites for photodegradation of IC dye under visible light. The prepared nanoparticles (NPs) have been characterized by various techniques and optimized composition was tested for degradation of IC dye in visible light.

2. Experimental Section

2.1. Materials

Zinc nitrate hexahydrate (Zn $(NO_3)_2.6H_2O$) (Sigma Aldrich), silver nitrate ($AgNO_3$) (Sigma Aldrich), and sodium hydroxide (NaOH) (Merck, Germany) were used as precursors in this experimental work, and the commercial indigo carmine (IC) dye produced by Alfa Aesar was used as a pollutant dye was used as supplied and its characteristics are depicted in Table 1. Double-distilled water (DDW) was used throughout the experiment. All the chemicals were used without further purification.

Table 1.: Characteristics of IC.

Dye	Chemical structure	Molecular formula	Molecular weight (g/mol)
Indigo carmine	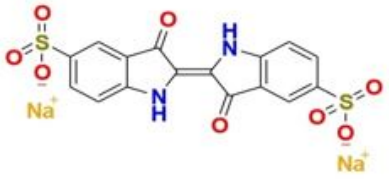	$C_{16}H_8N_2Na_2O_8S_2$	466.35

Table 1

2.2. Preparation of ZnO and Ag/ZnO nanocomposites:

The preparation of ZnO and Ag doped ZnO nanomaterials was carried out using the chemical co-precipitation method (Fig. 1). In a typical synthesis Zn $(NO_3)_2.6H_2O$ and NaOH were used as the starting materials. 40 ml aqueous solution of Zn $(NO_3)_2.6H_2O$ (0.1 M) with $AgNO_3$ (0, 1, 3, and 5 mol%) (Solution A) was prepared under mild stirring at 60 ^oC and 20 mL of sodium hydroxide (1 M) aqueous solution (Solution B) was added dropwise in solution A with constant stirring till pH ~ 12 was reached. The obtained solution was stirred magnetically for 2 hr to complete homogenization. After that, the resultant solution was kept overnight in order to settle down the NPs. The resultant products were centrifuged, washed multiple times using DDW, and ethanol. Finally, the materials were dried overnight at 60°C in a hot-air oven, and ZnO NPs were obtained by heat treatment at 500°C for 2 hr with a ramp rate of 10 $^0C\ min^{-1}$. Hereafter bare ZnO and Ag/ZnO samples with different mole percentages (1 mole%, 3 mole%, and 5 mole%) were referred to as AgZ-0, AgZ-1, AgZ-3, and AgZ-5 respectively.

Figure 1

2.3. Catalysts Characterization

The structural properties of the prepared materials were recorded by X-ray diffractometer (Rigaku SmartLab SE) in the 2θ range of 20 ^{0} – 80 ^{0} using Cu as a target (Cu K_α=1.5406 Å) at 45 kV and 40 mA. The morphology of bare ZnO and Ag (concentration = 1, 3, 5 mol%) doped ZnO were observed by scanning electron microscope (SEM – ZEISS EVO18) and high-resolution transmission electron microscopy (HRTEM, TEM – Thermofisher: Talos F200S G2). FTIR spectra were recorded on a ThermoFisher Scientific iS50 spectrometer. The Raman spectra of prepared nanomaterials were analyzed by Raman spectrometer (NOST: HEDA-URSM4/5/7). The charge transport properties of Ag/ZnO nanocomposites were studied using Novocontrol Alpha-A impedance analyzer. The data of UV–visible spectra were analyzed through a UV-Vis NIR

spectrophotometer (JASCO, V-670). The spectra of photoluminescence (PL) were provided by JASCO FP-8300 spectrofluorometer.

2.4. Detection of reactive species

Various scavenger tests were performed in the same way as activity evaluations in order to scrutinize the active species responsible for photodegradation of IC. For exploring the primary active species in the photocatalytic degradation of IC, potassium dichromate ($K_2Cr_2O_7$), ammonium oxalate ($C_2H_8N_2O_4$), isopropyl alcohol (C_3H_8O), p-benzoquinone ($C_6H_4O_2$) are used as an electron (e^-), holes (h^+), hydroxyl radicals (OH•), and superoxide radicals ($O_2^{\bullet -}$) scavengers.

2.5. Photocatalytic setup and Procedure

IC was utilized as a pollutant to estimate the photocatalytic activity of Ag/ZnO nanoparticles in a closed instrument. The photocatalytic studies were calculated under visible light illumination induced by lamps. A custom-built photoreactor system is made up of iron and degradation experiments were performed inside this reaction chamber. In the inner wall of reactor 12 fluorescent lamps of 100 W each were vertically installed (Fig. 2). For maintaining the temperature of reactor, two exhaust air circulating fans are provided at the exterior walls.
Figure 2

The degradation of IC dye (10 ppm concentration) was studied by taking 100 mL of dye in a glass beaker. The 0.1 g catalyst was dispersed in the 100 mL of aqueous IC dye solution. Before photocatalysis, the suspension was stirred constantly at 500 rpm using a magnetic stirrer in the dark for 30 min for attaining the adsorption-desorption mechanism between dye and catalyst. Later, the photodegradation efficiency was measured under visible light illumination by putting suspension in the custom-built reaction system. In the end, 3 mL of the suspension was collected after appropriate time intervals in order to measure IC concentration. The solution was centrifuged for 5 minutes at 2500 rpm and analyzed using a UV-Vis spectrophotometer. The degradation of IC dye was obtained by observing a decrease in the absorption characteristics band intensity at 610 nm. The percentage degradation was calculated using Eq. (1) (Janbandhu et al. 2018):

$$\%\text{Degradation} = \frac{C_0 - C}{C} \times 100 \quad (1)$$

where C_0 and C correspond to the concentration of IC dye solution at time 0 (after dark adsorption) and t respectively.

3. Results And Discussion

3.1. XRD analysis

Figure 3(a) illustrates the XRD patterns of samples AgZ-0, AgZ-1, AgZ-3, and AgZ-5. The majority of the diffraction peaks in Fig. 3 (a) can ascribe to zinc oxide (JCPDS: 01-076-0704), whereas the peaks marked with as # can be assigned to Ag (JCPDS: 01-087-0717). All diffraction peaks in the XRD patterns reveal the presence of hexagonal wurtzite phase of ZnO, space group: $P^6{}_3mc$, a = 3.2530 Å, c = 5.2130 Å), with preferential growth along (101) crystal plane. No additional peaks were observed in the case of 1% Ag doping due to its low concentration and high dispersity (Chelli and Golder 2018). However, some additional peaks were observed for the samples with Ag concentration (≥ 3%) and are indexed as (111), (200), and (220) crystal planes of cubic silver (Sun et al. 2012). It was observed that the position of (101) peak slightly shifts towards higher 2θ values with the increasing Ag doping concentration (Fig. 3(b)). As a result of the difference in the ionic radii of Zn^{2+} (0.074 nm), and Ag^+ (0.122 nm), stress is produced at the boundaries and edges of the host lattice during the growth and formation process (Raji et al. 2018). The mean crystallite sizes of the nanoparticles were calculated from the XRD data with the Scherrer equation:

$$D_{hkl} = \frac{K\lambda}{\beta \mathrm{Cos}\theta}$$

2

where $D_{hkl}$is the crystallite size, where λ = 1.5406 Å, $\beta$and θ indicates the wavelength, full width at half maximum (FWHM), and the Bragg angle respectively.

The calculated values of crystallite size are depicted in Table 2. From this table, it is observed that the crystallite size increases with increase in Ag content. This increase in crystallite size was due to the segregation of Ag species on the grain boundaries of ZnO crystallites, or an insignificant amount of Ag atoms would have incorporated into the lattice of ZnO (Georgekutty et al. 2008; Chauhan et al. 2020). These results support the shifting of (101) diffraction peak towards higher 2θ value.

Table 2
Variation of crystallite size and band gap for the synthesized Ag/ZnO nanocomposites.

Sample ID	Ag concentration (mole%)	Average crystallite size (nm)	Band gap (eV)
AgZ-0	0	26.21	3.17
AgZ-1	1	26.36	3.16
AgZ-3	3	27.43	3.13
AgZ-5	5	27.83	3.12

Figure 3

Table 2

3.2. SEM and TEM analysis

SEM was used to examine the morphology of Ag/ZnO nanocomposites. Figure 4. shows SEM micrographs of (a) AgZ-0, (b) AgZ-1, (c) AgZ-3 and (d) AgZ-5 respectively. From the SEM micrographs, irregular and non-uniform size of NPs was observed. The low resolution SEM images suggest that the NPs are agglomerated with each other and the size of these NPs was increased with the increase in doping concentration.

Figure 4

HRTEM measurements were conducted to investigate the particle size and morphological characteristics of AgZ-5. Figure 5(a) shows the high magnification TEM images of AgZ-5, which exhibits nanoparticles like morphology. The observed nanoparticles were spherical in nature with hexagonal shape. The corresponding SAED pattern (Fig. 5(b)) of Ag/ZnO heterostructures exhibit reflections (002), (101), (102), (103), (112) corresponding to the hexagonal wurtzite phase of ZnO particles along with the (111) diffraction lines of Ag. Figure 5(c) depicts the HRTEM image of the AgZ-5, which shows 0.21 nm lattice fringes belong to plane (111) of fcc Ag at the edge portion and 0.19 nm fringes belonging to plane (102) of hexagonal-type wurtzite ZnO at the edge portion, confirming crystallinity of Ag and ZnO components at the edge portion. The particle size of AgZ-5 was determined by combining several crystallites and was fitted with Gaussian distribution (Fig. 5(d)). It appeared that particle size was greater than crystallite size. The standard ImageJ software was used to estimate the size of AgZ-5 nanoparticles, and the average particle size was found to be 29.82 nm.

Figure 5

EDS is a common scientific technique for analyzing the elemental composition of a specimen. In order to analyze formation of pure nanocomposite without other impurities, energy dispersive spectroscopy (EDS) with a HRTEM was used, and it revealed peaks only associated with Zn, Ag, and O (Fig. 6). The observed atomic percentages of Zn, O, and Ag in nanocomposite were 48.46%, 51.23%, and 0.29% respectively.

Figure 6

3.3. FTIR Spectroscopic studies

FTIR spectra of the prepared nanocomposites was recorded in the range of 400–4000 cm^{-1}, and it is given in Fig. 7(a). A significant vibration band in the FTIR spectrum is assigned to the characteristic stretching mode of the ZnO bond ranging from 400 cm^{-1} to 500 cm^{-1} (Gayathri1 et al. 2015). A similar spectra profile can be observed for all Ag/ZnO samples with different band positions due to addition of Ag content in ZnO. In FTIR spectra, there is a broad peak at ~ 3434 cm^{-1} (stretching) and ~ 1330 cm^{-1} to ~ 1670 cm^{-1} (bending) which confirms the presence of hydroxyl residues due to stretching. These bands are due to the stretching mode of the O-H group (Nagaraju et al. 2017).

Figure 7

3.4. Raman Spectroscopy

Raman spectroscopy is a very useful tool to find the structural disorder and defects in the prepared samples. For Raman spectroscopy, Group theory predicts that wurtzite ZnO features the following characteristic optical phonon modes:

$\Gamma = 1A_1 + 2B_1 + 1E_1 + 2E_2$

where A_1 and E_1 modes are polar and these split into transverse (TO) and longitudinal optical (LO) phonons (Zhang et al. 2009). The phonon modes of Raman active (A1, E1, and E2) and infrared active (A1 and E1) were observed. (Lupan et al. 2010). But the B_1 modes are infrared and Raman inactive and are normally silent modes (Sánchez Zeferino et al. 2011).

The Raman spectra of all four samples was shown in Fig. 7(b). The Raman spectra of all the nanocomposites were taken in the frequency range of 50 to 800 cm^{-1}. The dominant peaks of pristine ZnO at ~ 99 and ~ 436 cm^{-1} are associated with the vibration of Zn and O atoms in the ZnO lattice, respectively. These peaks are attributed to the low and high E_2 mode (E_{2L} and E_{2H}) of nonpolar optical phonons while the peaks around 380 and 574 cm^{-1} correspond to A_1(TO) and A_1(LO) fundamental modes of hexagonal ZnO respectively. The Raman bands at ~ 406 cm^{-1} reflecting the strength of the polar lattice bonds are assigned to the E_1(TO) modes. While the peak at about ~ 330 cm^{-1} corresponds to multiphonon scattering mode (Udayabhaskar et al. 2015; Sawant et al. 2018).

3.5. Impedance study

The impedance studies of the prepared materials have been recorded. The respective Nyquist plots are shown in Fig. 8 along with the equivalent circuit. An equivalent circuit contains a series resistance (R_s), a charge transfer resistance (R_{ct}), and a capacitor (Dridi et al. 2018). The electrochemical charge transfer resistances of the prepared materials were found to decrease with the addition of Ag and was minimal for the AgZ-5 sample. As a result, the spatial separation and transport of photogenerated e^--h^+ pairs is maximum in AgZ-5.

Figure 8

3.6. Absorption study

Figure 9(a) demonstrates the UV-Vis DRS absorption spectra of the ZnO containing various proportions of silver. The absorption spectra of Ag/ZnO NPs show enhanced absorbance in the visible region as compared to bare ZnO, this is most likely owing to a strong interfacial electron coupling between Ag NPs and ZnO. The prepared Ag/ZnO nanoparticles can efficiently utilize light for organic pollutant photodegradation because of the broad absorption in the visible range (Raji et al. 2018). This increased absorbance is due to the surface plasmon resonance (SPR) of Ag NPs.

Figure 9

The optical band gap (E_g) of the prepared photocatalysts was estimated using Tauc's equation as follows (Sukhadeve et al. 2021):

$\alpha h\nu = A\,(h\nu - E_g)^n$ (3)

where α - absorption coefficient, hν – energy of photon, A - constant, E_g - optical energy band gap, n - depends on the transition (n = 1/2, 2 corresponding to allowed direct, allowed indirect transitions respectively) (Janbandhu et al. 2019b).

The band gap of all samples was estimated by plotting the $(\alpha h\nu)^2$ and photon energy (hν). The bandgap was obtained by extrapolating the tangential line of x-axis intercept from the linear region of the plot (Fig. 9(b)) and shown in Table 1. It is observed from this table that, energy band gap of Ag/ZnO NPs decreases with an increase in Ag content. This reduction in energy band gap may be due to the increase in crystallite size.

3.7. Photoluminescence measurement

Photoluminescence spectroscopy is a well known technique to study electronic structure, impurities, and recombination rate of free carriers of semiconductor materials. Figure 10 depicts the PL spectra recorded at room temperature for bare ZnO and Ag/ZnO nanoparticles with the excitation wavelength of 325 nm. A number of peaks were observed in the 335–650 nm range spanning both UV and visible regions. The narrow emission in the UV range is due to free exciton recombination. Although emission in the visible region was due to the defects like oxygen vacancies, zinc interstitials, etc. From Fig. 10, PL intensity was found to be decreased with an increase in Ag doping in ZnO. The doping of Ag in ZnO acts as a trap for photogenerated e^- which reduces the recombination of e^- - h^+ pairs resulting in lower PL intensity as compared to bare ZnO (Chitradevi et al. 2019). The PL intensity for AgZ-5 is found to be lowest among all due to lower recombination of photogenerated e^- - h^+ pairs, and therefore it can be used for photocatalytic performance (Sarma and Sarma 2017; Sukhadeve et al. 2021). The results observed from PL are also in good agreement with the impedance study.

Figure 10

3.8. Photocatalytic degradation activity of IC dye

The effectiveness of Ag/ ZnO nanocomposites for the IC dye degradation were studied under visible light illumination. It was observed that the photocatalytic activity was improved as the Ag concentration increased. The intensity of the absorption peaks was gradually decreased after every time interval (Fig. 11(a)). The decrease in dye concentration under light illumination indicates that Ag/ZnO nanocomposites are a promising group of photocatalysts for IC dye degradation (Fig. 11(b)).

Figure 11

To get more quantitative insight, the kinetic study was done for the photocatalytic activity of Ag/ZnO nanocomposites. The pseudo-first order law gives rate constant of photocatalytic reaction (Chen et al. 2017; Raza et al. 2019) and is depicted in Table 3.

Table 3
Photocatalytic degradation of IC dye.

Photocatalyst	Dye	Degradation time (min)	% Degradation	k (min^{-1})	$T_{1/2}$ (min^{-1})	Adj-R^2
AgZ-0	IC	120	72.20	0.00857	80.88	0.9698
AgZ-1	IC	120	75.20	0.00900	77.02	0.9376
AgZ-3	IC	120	79.09	0.00953	72.73	0.9399
AgZ-5	IC	120	95.71	0.01957	35.42	0.9299

$$\ln\frac{C}{C_0} = \text{kt (4)}$$

where k is the reaction rate constant, and t is irradiation time.

Figure 11(c) shows a plot of -ln(C/C_0) vs. the irradiation time, which suggests that the degradation of IC by Ag/ZnO nanocomposites follows pseudo-first order kinetics. The calculated rate constants (k) for all samples are as follows: AgZ-0 (0.00857 min^{-1}), AgZ-1 (0.00900 min^{-1}), AgZ-3 (0.00953 min^{-1}) and, AgZ-5 (0.01957 min^{-1}). From Table 3, it is observed that the rate constant of AgZ-5 was significantly higher than that of AgZ-0, which indicates that the photocatalytic reaction was faster in the AgZ-5 sample. In addition, the degradation efficiency was calculated for all the prepared samples. It was observed that the nanocomposites AgZ-0, AgZ-1, and AgZ-3 have a moderate effect on degradation efficiency of IC and the percentage degradation efficiency of these photocatalysts was 72.20%, 75.20%, and 79.09%, respectively. In contrast, nanocomposite AgZ-5 had a considerable effect on the photodegradation of IC and gives a degradation efficiency of 95.71% during the span of 120 minutes (Fig. 11(d)). Consequently, among all the samples AgZ-5 sample had the greatest rate constant, and also had the highest photocatalytic effectiveness of 95.71% degradation towards IC dye.

For the prepared samples, efficiency for IC dye degradation, and rate constant (k) were calculated and shown in Table 3. The half life period of first order reaction is the time required for 50% completion of reaction. For the prepared samples, half life was calculated by using following equation:

Half life period = $\frac{ln(2)}{k}$ (5)

The calculated half life period for samples is depicted in Table 3. From this table, it is observed that half life period is found to be minimum (35.42 min^{-1}) for AgZ-5 sample.

Table 3

In addition, the observed results of AgZ-5 are compared with the available literature (Table 4) and found the prepared sample is more efficient for IC dye degradation.

Table 4
Comparison of our results with the other photocatalysts.

S. No.	Method	Material	Pollutant (Concentration)	Source	Catalyst	Time (min)	Efficiency	References
1	SILAR	ZnO: Ag 5wt%	MB (10 mg/L)	UV light	50 mg	180 min	75.8%	[37]
2.	Chemical precipitation method	Ce–ZnO	MO (5 mg/L)	High-pressure mercury lamp (250 W)	500 mg	240 min	89.5%	[38]
3.	Electrospinning method	Fe–ZnO	MB (10 mg/L)	Mercury lamp	400 mg	360 min	88%	[39]
4.	Sol gel method	Ag-doped ZnO	MB (10 mg/L)	Visible light	NM	140 min	45.1%	[40]
5.	Sol–gel spin coating technique	Ag/ZnO NPs nanocomposite thin films	IC (6.6 mg/L)	Visible light	NM	441 min	NM	[41]
6.	Spray pyrolysis	ZnO/Bi_2O_3 heterostructures thin films	IC (5 mg/L)	Visible light	NM	720 min	NM	[42]
7.	Chemical bath deposition method	ZnO nanorod ZnO nanoflower	IC (10 mg/L) IC (10 mg/L)	Visible light Visible light	NM	720 min	~14% 9%.	[43] [43]
8.	Sol-gel	Ag/GO/ZnO	MB (15 mg/L)	100 W UV lamp	300 mg	180 min	97.5%	[44]
9.	Co-precipitation method	Ag/ZnO nanocomposites	IC (10 mg/L)	Visible light	100 mg	120 min	95.71%	Present study

* NM- not mentioned

Table 4

3.9. Possible photocatalytic mechanism and trapping studies

Bare ZnO showed limited photodegradation under the visible light irradiation whereas Ag/ZnO nanocomposites showed significantly higher degradation as the Ag concentration was increased. The limited visible-light photocatalytic activity of bare ZnO was due to the presence of oxygen vacancies. While the enhanced photocatalytic activity mechanism of Ag/ZnO towards IC dye degradation under visible light irradiation can be understood as follows:

The photocatalytic activity of Ag/ZnO nanocomposites was enhanced significantly because the doping of Ag in ZnO leads to the formation of Schottky barrier at the surface of Ag and ZnO. This Schottky barrier was developed due to the difference in the work functions of Ag (~ 4.2 eV) and bare ZnO nanoparticles (~ 5.3 eV) (Raji et al. 2018). However, due to the strong electron oscillation by surface plasmon resonance (SPR) excitation, it has been observed that electrons can migrate from Ag to the conduction band of ZnO. Generally, electrons are transported from a substance with a lower work function to one with a higher work function until they reach an equilibrium point for the formation of fermi level (Liu et al. 2015). Furthermore, the Schottky barrier generated at the Ag/ZnO interface can inhibit electron transmission from Ag to ZnO. The migrated electrons are scavenged by adsorbed oxygen to form highly oxidative species such as $O_2^{\bullet -}$. As a result, these reactive $O_2^{\bullet -}$ cause IC to

degrade. Meanwhile, Ag on the ZnO surface may also function as an electron scavenger by transferring photo-excited electrons from the oxygen vacancy ($V_O^{\bullet\bullet}$) defect level of ZnO to the E_f of Ag.

Further information on Ag/ZnO semiconductors with photocatalytic potential can be understood by VB and CB potential analyses. The CB and VB edge potentials can be calculated by Mullikens electronegativity equations (6) and (7) at the normal hydrogen electrode potential (E_e, NHE = 4.5 eV), and the band gap value (E_g):

$$E_{(CB)} = \chi - E_e - 0.5\, E_g \quad (6)$$

$$E_{(VB)} = E_{(CB)} + E_g \quad (7)$$

Where χ is the absolute electronegativity, E_g is the band gap energy of the semiconductor, and E_{VB} and E_{CB} are the VB and CB edge potentials respectively. Moreover, E_e represents the energy of free electrons which is ~ 4.5 eV on the hydrogen scale and χ is the geometric mean of absolute Mulliken electronegativity having a value of ~ 5.4 eV for ZnO semiconductor (Janbandhu et al. 2019a). The value of E_{CB} and E_{VB} were calculated and found to be − 0.27 eV and 2.85 eV, respectively. Here, the CB of Ag/ZnO nanocomposites has a lower redox potential than O_2/ $O_2^{\bullet -}$ (-0.33) eV, which indicates that O_2 cannot be reduced to $O_2^{\bullet -}$ (Nosaka and Nosaka 2017). But holes have enough positive redox potential because the oxidation potential of H_2O/ $OH^{\bullet -}$ is 2.27 eV, so holes oxidize surface hydroxyl ions into OH• radicals in the valence band (Liu et al. 2019). On the basis of these explanations, we have proposed a possible mechanism for the degradation of IC dye by Ag/ZnO nanocomposites and which is shown in Fig. 12 (a).

Figure 12

The corresponding reaction mechanism is demonstrated as follows (equations 8 to 13):

$$Ag/ZnO + hv \rightarrow Ag/ZnO\ (e^- + h^+) \quad (8)$$

$$e^- + O_2 \rightarrow O_2^{\bullet -} \quad (9)$$

$$Ag^+ + e^-\ (CB) \rightarrow Ag \quad (10)$$

$$h^+ + OH^- \rightarrow OH^\bullet \quad (11)$$

$$OH^\bullet + \text{IC dye} \rightarrow \text{degradation products} \quad (12)$$

$$O_2^{\bullet -} + \text{IC dye} \rightarrow \text{degradation products} \quad (13)$$

To better understand the underlying mechanism involved in the degradation process radical capture experiments were performed. The benzoquinone (BQ) was adopted to scavenge superoxide radical ($O_2^{\bullet -}$), ammonium oxalate (AO) was selected to trap h^+, potassium dichromate (PD) was introduced to trap e^-, and isopropanol (IPA) was adopted to quench the hydroxyl radical (OH•). Figure 12(b) shows the rate of IC degradation over photocatalysts in the presence of scavengers. The addition of AO and BQ drastically reduces the rate of IC removal. Based on the above trapping experiments, it was found that the h^+ species were mostly responsible for degradation of IC dye. The $O_2^{\bullet -}$ have a secondary role in the degradation, whereas the contribution of hydroxyl radicals is negligible.

4. Conclusions

In summary, we have prepared Ag/ZnO nanocomposites by a simple co-precipitation method. XRD, SEM, HRTEM-EDS, UV-Visible, FTIR, Raman, Impedance spectroscopy and photoluminescence analysis were used to characterize the prepared photocatalysts. The UV-Vis study reveals that the SPR effect of Ag nanoparticles causes increased absorbance in the visible

region. With the increase of Ag doping concentration, the photocatalytic efficiency was improved, and also the rate constant is higher than that of bare ZnO. Our experimental results suggest that the 5 mole% Ag/ZnO photocatalyst shows better results compared to other prepared photocatalysts. More specifically, the photocatalytic efficiency of the 5 mole% Ag/ZnO was 95.71% in a 120 min reaction time. Consequently, the prepared photocatalyst materials are suitable for the degradation of IC dye. It has been revealed that the improved photocatalytic efficiency was due to the enhanced charge transfer between ZnO and Ag and their synergistic effect. Also, the quencher study analysis indicates that the h^+ and $O_2^{\bullet -}$ radical play an important role to degrade the IC dye. The improved photocatalytic activity of the developed photocatalyst shows that it is effective under visible light irradiation and could be useful for organic pollutant degradation.

Declarations

Acknowledgments RK gratefully acknowledges the Director VNIT, Nagpur for providing the financial support. The authors express sincere thanks to DST-FIST, New Delhi (GOI) for instrumentation facility under the FIST program (No. SR/FST/PSI/2017/5(C)). We are also thankful to the CeNS Bengaluru who generously made HRTEM characterization available facility to undertake this work. Our thanks are also extended to the Department of Physics, R.T.M. Nagpur University.

Authors Contributions Rahul Kumar: Methodology, Formal analysis, Investigation, Visualization, Writing – original draft, Writing – review & editing. Shaileshkumar Y. Janbandhu: Conceptualization, Methodology, Formal analysis. Gaurav K. Sukhadeve: Resources, Writing review & editing. Rupesh S. Gedam: Conceptualization, Investigation, Resources, Writing-review & editing, Supervision.

Funding Not applicable.

Availability of data and materials All data and materials in this study are included in this article.

Ethical approval The manuscript is not submitted to any other journal.

Consent of participate Not applicable.

Consent to publication The submitted work is original.

Conflict of interest The authors declare no competing interests.

References

1. Bueno-Alejo CJ, Graus J, Arenal R et al (2021) Anisotropic Au-ZnO photocatalyst for the visible-light expanded oxidation of n-hexane. Catal Today 362:97–103. https://doi.org/https://doi.org/10.1016/j.cattod.2020.03.063
2. Chaudhary A, Malik P, Mehra R, Raina KK (2013) Influence of ZnO nanoparticle concentration on electro-optic and dielectric properties of ferroelectric liquid crystal mixture. J Mol Liq 188:230–236. https://doi.org/https://doi.org/10.1016/j.molliq.2013.09.020
3. Chauhan A, Verma R, Kumari S et al (2020) Photocatalytic dye degradation and antimicrobial activities of Pure and Ag-doped ZnO using Cannabis sativa leaf extract. Sci Rep 10:1–16. https://doi.org/10.1038/s41598-020-64419-0
4. Chelli VR, Golder AK (2018) Ag-doping on ZnO support mediated by bio-analytes rich in ascorbic acid for photocatalytic degradation of dipyrone drug. Elsevier Ltd
5. Chen X, Wu Z, Liu D, Gao Z (2017) Preparation of ZnO Photocatalyst for the Efficient and Rapid Photocatalytic Degradation of Azo Dyes. Nanoscale Res Lett 12:143. https://doi.org/10.1186/s11671-017-1904-4
6. Chitradevi T, Jestin Lenus A, Victor Jaya N (2019) Structure, morphology and luminescence properties of sol-gel method synthesized pure and Ag-doped ZnO nanoparticles. Mater Res Express 7. https://doi.org/10.1088/2053-1591/ab5c53

7. Dridi D, Bouaziz L, Karyaoui M et al (2018) Effect of silver doping on optical and electrochemical properties of ZnO photoanode. J Mater Sci Mater Electron 29:8267–8278. https://doi.org/10.1007/s10854-018-8835-4
8. Elango G, Roopan SM (2016) Efficacy of SnO2 nanoparticles toward photocatalytic degradation of methylene blue dye. J Photochem Photobiol B Biol 155:34–38. https://doi.org/https://doi.org/10.1016/j.jphotobiol.2015.12.010
9. Gao P, Ng K, Sun DD (2013) Sulfonated graphene oxide–ZnO–Ag photocatalyst for fast photodegradation and disinfection under visible light. J Hazard Mater 262:826–835. https://doi.org/https://doi.org/10.1016/j.jhazmat.2013.09.055
10. Gayathri1 S, Sivaraman O, Ghosh1 N et al (2015) Investigation of physicochemical properties of Ag doped ZnO nanoparticles prepared by chemical route. Appl Sci Lett 1:8–13
11. Georgekutty R, Seery MK, Pillai SC (2008) A Highly Efficient Ag-ZnO Photocatalyst: Synthesis, Properties, and Mechanism. J Phys Chem C 112:13563–13570. https://doi.org/10.1021/jp802729a
12. Guo Q, Zhou C, Ma Z, Yang X (2019) Fundamentals of TiO2 Photocatalysis: Concepts, Mechanisms, and Challenges. Adv Mater 31:1–26. https://doi.org/10.1002/adma.201901997
13. Janbandhu SY, CT S, Munishwar SR et al (2022) Borosilicate glasses containing CdS/ZnS QDs: A heterostructured composite with enhanced degradation of IC dye under visible-light. Chemosphere 286:131672. https://doi.org/10.1016/j.chemosphere.2021.131672
14. Janbandhu SY, Joshi A, Munishwar SR, Gedam RS (2019a) CdS/TiO2 heterojunction in glass matrix: Synthesis, characterization, and application as an improved photocatalyst. Appl Surf Sci 497:143758. https://doi.org/https://doi.org/10.1016/j.apsusc.2019.143758
15. Janbandhu SY, Munishwar SR, Gedam RS (2018) Synthesis, characterization and photocatalytic degradation efficiency of CdS quantum dots embedded in sodium borosilicate glasses. Appl Surf Sci 449:221–227. https://doi.org/https://doi.org/10.1016/j.apsusc.2018.02.065
16. Janbandhu SY, Munishwar SR, Sukhadeve GK, Gedam RS (2019b) Effect of annealing time on optical properties of CdS QDs containing glasses and their application for degradation of methyl orange dye. Mater Charact 152:230–238. https://doi.org/https://doi.org/10.1016/j.matchar.2019.04.027
17. Jaramillo-Páez CA, Navío JA, Hidalgo MC, Macías M (2018) ZnO and Pt-ZnO photocatalysts: Characterization and photocatalytic activity assessing by means of three substrates. Catal Today 313:12–19. https://doi.org/https://doi.org/10.1016/j.cattod.2017.12.009
18. Kumari V, Yadav S, Mittal A et al (2020) Surface Plasmon response of Pd deposited ZnO/CuO nanostructures with enhanced photocatalytic efficacy towards the degradation of organic pollutants. Inorg Chem Commun 121:108241. https://doi.org/https://doi.org/10.1016/j.inoche.2020.108241
19. Lee KM, Lai CW, Ngai KS, Juan JC (2016) Recent developments of zinc oxide based photocatalyst in water treatment technology: A review. Water Res 88:428–448. https://doi.org/https://doi.org/10.1016/j.watres.2015.09.045
20. Lellis B, Fávaro-Polonio CZ, Pamphile JA, Polonio JC (2019) Effects of textile dyes on health and the environment and bioremediation potential of living organisms. Biotechnol Res Innov 3:275–290. https://doi.org/https://doi.org/10.1016/j.biori.2019.09.001
21. Li S, Cai J, Wu X, Zheng F (2018) Sandwich-like TiO2@ZnO-based noble metal (Ag, Au, Pt, or Pd) for better photo-oxidation performance: Synergistic effect between noble metal and metal oxide phases. Appl Surf Sci 443:603–612. https://doi.org/https://doi.org/10.1016/j.apsusc.2018.03.017
22. Liu H, Hu Y, Zhang Z et al (2015) Synthesis of spherical Ag/ZnO heterostructural composites with excellent photocatalytic activity under visible light and UV irradiation. Appl Surf Sci 355:644–652. https://doi.org/10.1016/j.apsusc.2015.07.012
23. Liu P, Yi J, Bao R, Fang D (2019) A flower-like Zn3V2O8/Ag composite with enhanced visible light driven photocatalytic activity: The triple-functional roles of Ag nanoparticles. New J Chem 43:7482–7490. https://doi.org/10.1039/c9nj00211a

24. Lupan O, Chow L, Ono LK et al (2010) Synthesis and characterization of ag- or sb-doped zno nanorods by a facile hydrothermal route. J Phys Chem C 114:12401–12408. https://doi.org/10.1021/jp910263n
25. Nagaraju G, Udayabhanu, Shivaraj et al (2017) Electrochemical heavy metal detection, photocatalytic, photoluminescence, biodiesel production and antibacterial activities of Ag–ZnO nanomaterial. Mater Res Bull 94:54–63. https://doi.org/10.1016/j.materresbull.2017.05.043
26. Nosaka Y, Nosaka AY (2017) Generation and Detection of Reactive Oxygen Species in Photocatalysis. Chem Rev 117:11302–11336. https://doi.org/10.1021/acs.chemrev.7b00161
27. Raji R, Sibi KS, Gopchandran KG (2018) ZnO:Ag nanorods as efficient photocatalysts: Sunlight driven photocatalytic degradation of sulforhodamine B. Appl Surf Sci 427:863–875. https://doi.org/10.1016/j.apsusc.2017.09.050
28. Raza W, Haque MM, Muneer M, Bahnemann D (2019) Synthesis of visible light driven TiO2 coated carbon nanospheres for degradation of dyes. Arab J Chem 12:3534–3545. https://doi.org/https://doi.org/10.1016/j.arabjc.2015.09.002
29. Sánchez Zeferino R, Barboza Flores M, Pal U (2011) Photoluminescence and raman scattering in ag-doped zno nanoparticles. J Appl Phys 109. https://doi.org/10.1063/1.3530631
30. Saravanan R, Mansoob Khan M, Gupta VK et al (2015) ZnO/Ag/CdO nanocomposite for visible light-induced photocatalytic degradation of industrial textile effluents. J Colloid Interface Sci 452:126–133. https://doi.org/https://doi.org/10.1016/j.jcis.2015.04.035
31. Sarma B, Sarma BK (2017) Fabrication of Ag/ZnO heterostructure and the role of surface coverage of ZnO microrods by Ag nanoparticles on the photophysical and photocatalytic properties of the metal-semiconductor system. Appl Surf Sci 410:557–565. https://doi.org/https://doi.org/10.1016/j.apsusc.2017.03.154
32. Sawant SY, Kim JY, Han TH et al (2018) Electrochemically active biofilm-assisted biogenic synthesis of an Ag-decorated ZnO@C core-shell ternary plasmonic photocatalyst with enhanced visible-photocatalytic activity. New J Chem 42:1995–2005. https://doi.org/10.1039/c7nj03936k
33. Sukhadeve G, Shaileshkumar, Janbandhu Y et al (2021) Ag-Doped TiO 2 Nanoparticles as an Effective Photocatalyst for Degradation of Indigo Carmine Dye under Visible Light. ChemistrySelect 6:12873–12883. https://doi.org/10.1002/slct.202103629
34. Sukhadeve GK, Janbandhu SY, Upadhyay S, Gedam RS (2022) Investigation of photocatalytic activity of TiO2 nanoparticles synthesized by sol–gel technique. J Aust Ceram Soc 58:39–48. https://doi.org/10.1007/s41779-021-00658-2
35. Sun F, Qiao X, Tan F et al (2012) One-step microwave synthesis of Ag/ZnO nanocomposites with enhanced photocatalytic performance. J Mater Sci 47:7262–7268. https://doi.org/10.1007/s10853-012-6676-8
36. Udayabhaskar R, Mangalaraja RV, Karthikeyan B (2015) Enhanced Fluorescence, Raman Scattering, and Higher Order Raman Modes in ZnO:Ag Nanorods. Plasmonics 10:893–899. https://doi.org/10.1007/s11468-015-9877-6
37. Zhang R, Yin P-G, Wang N, Guo L (2009) Photoluminescence and Raman scattering of ZnO nanorods. Solid State Sci 11:865–869. https://doi.org/https://doi.org/10.1016/j.solidstatesciences.2008.10.016
38. Zhang X, Wang Y, Hou F et al (2017) Effects of Ag loading on structural and photocatalytic properties of flower-like ZnO microspheres. Appl Surf Sci 391:476–483. https://doi.org/10.1016/j.apsusc.2016.06.109
39. Zhang X, Zhao J, Wang S et al (2014) Shape-dependent localized surface plasmon enhanced photocatalytic effect of ZnO nanorods decorated with Ag. Int J Hydrogen Energy 39:8238–8245. https://doi.org/https://doi.org/10.1016/j.ijhydene.2014.03.153

Figures

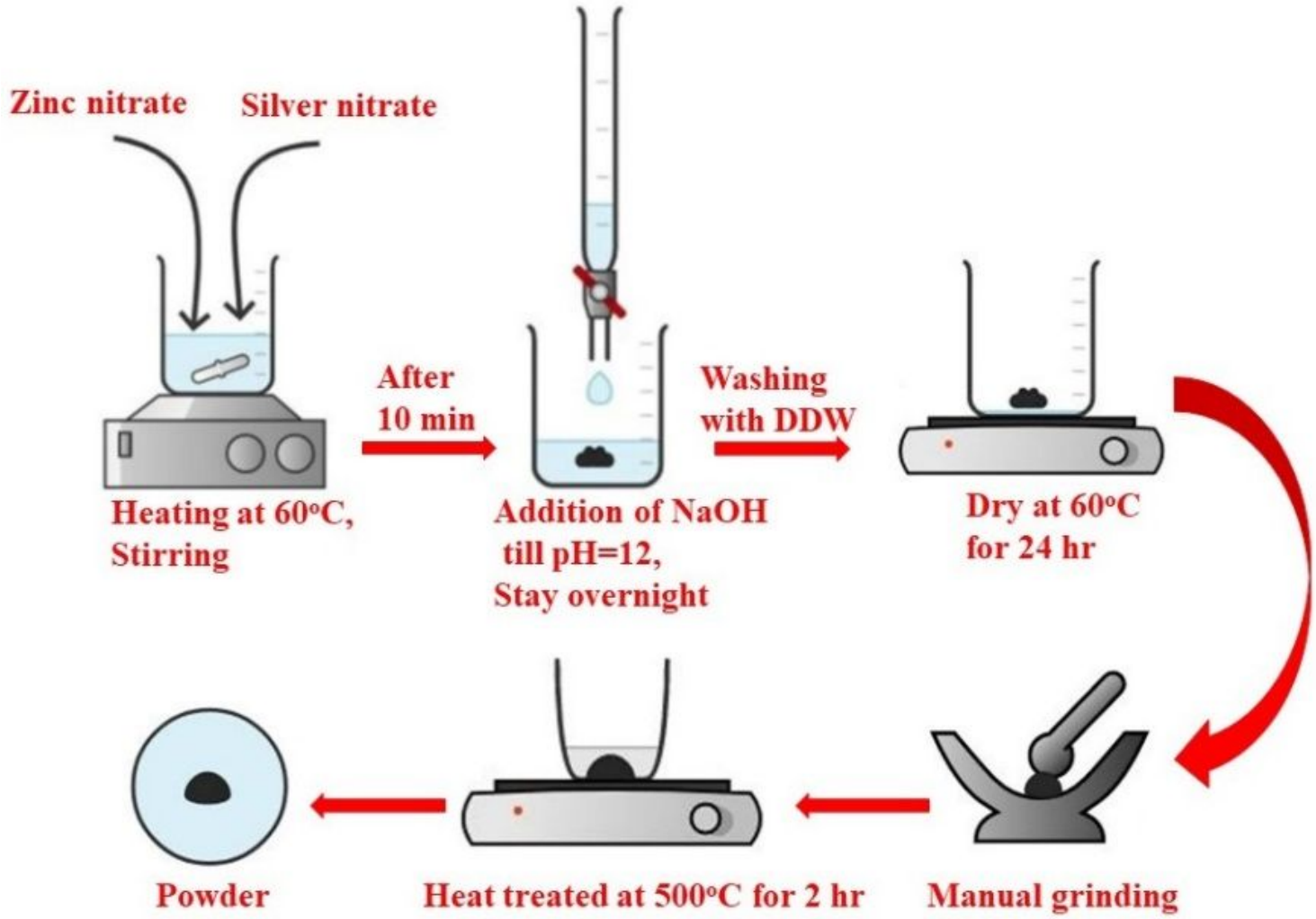

Figure 1

Schematic illustration of the reaction process for the synthesis of Ag/ZnO nanocomposites.

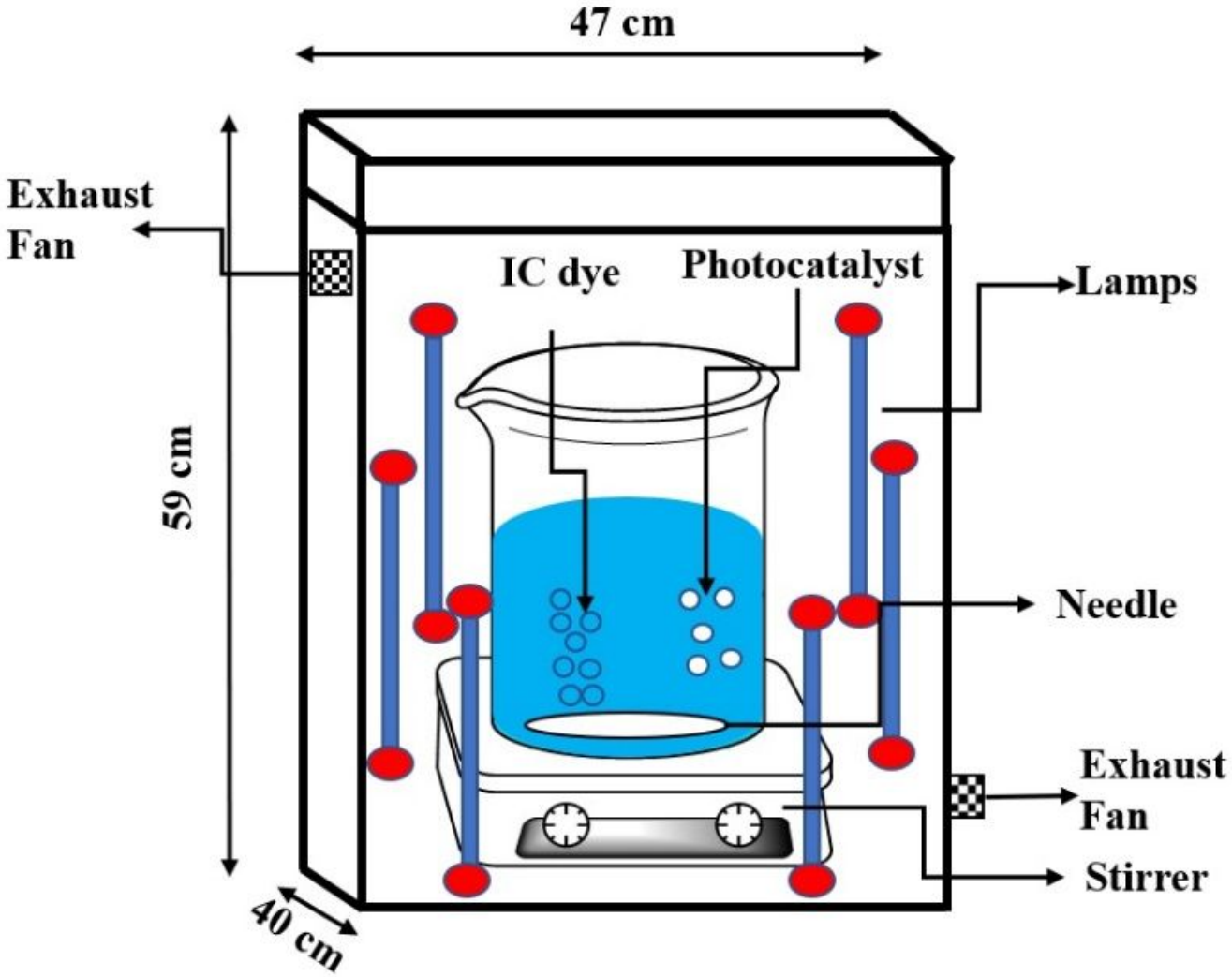

Figure 2

Schematic layout of the systematically designed photoreactor system.

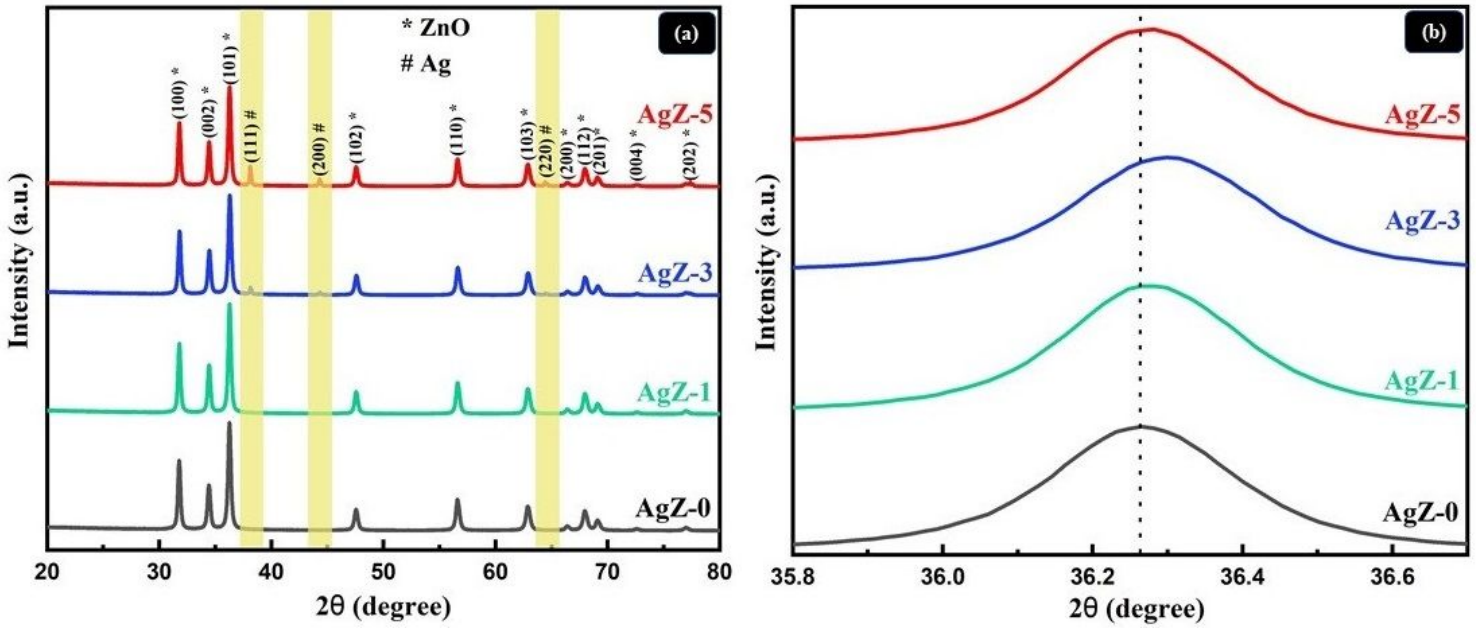

Figure 3

(a) XRD patterns of AgZ-0, AZ-1, AZ-3, and AZ-5 photocatalysts, and (b) Enlarged XRD of (101) peak.

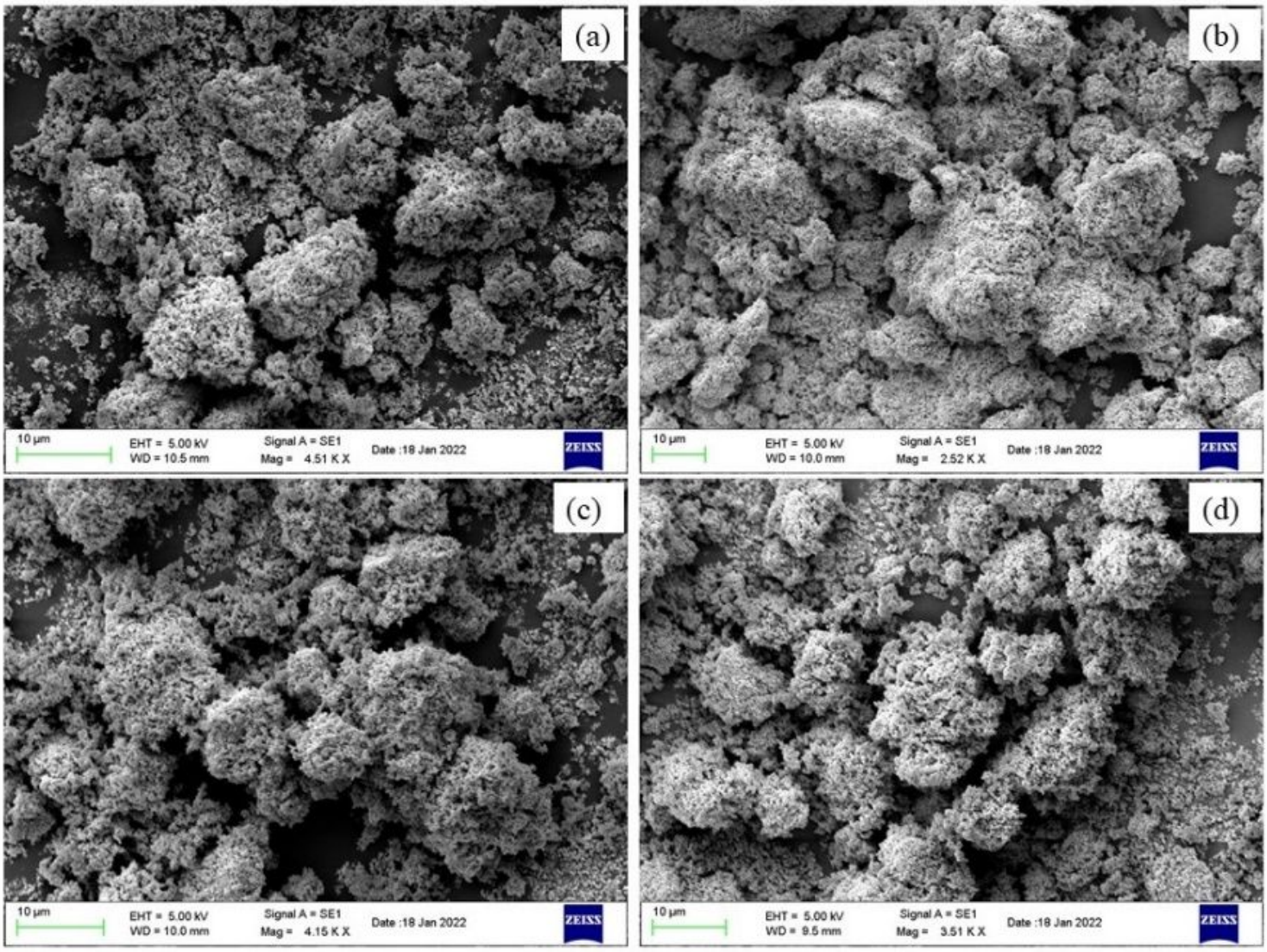

Figure 4

SEM micrographs of (a) AgZ-0, (b) AgZ-1, (c) AgZ-3, and (d) AgZ-5.

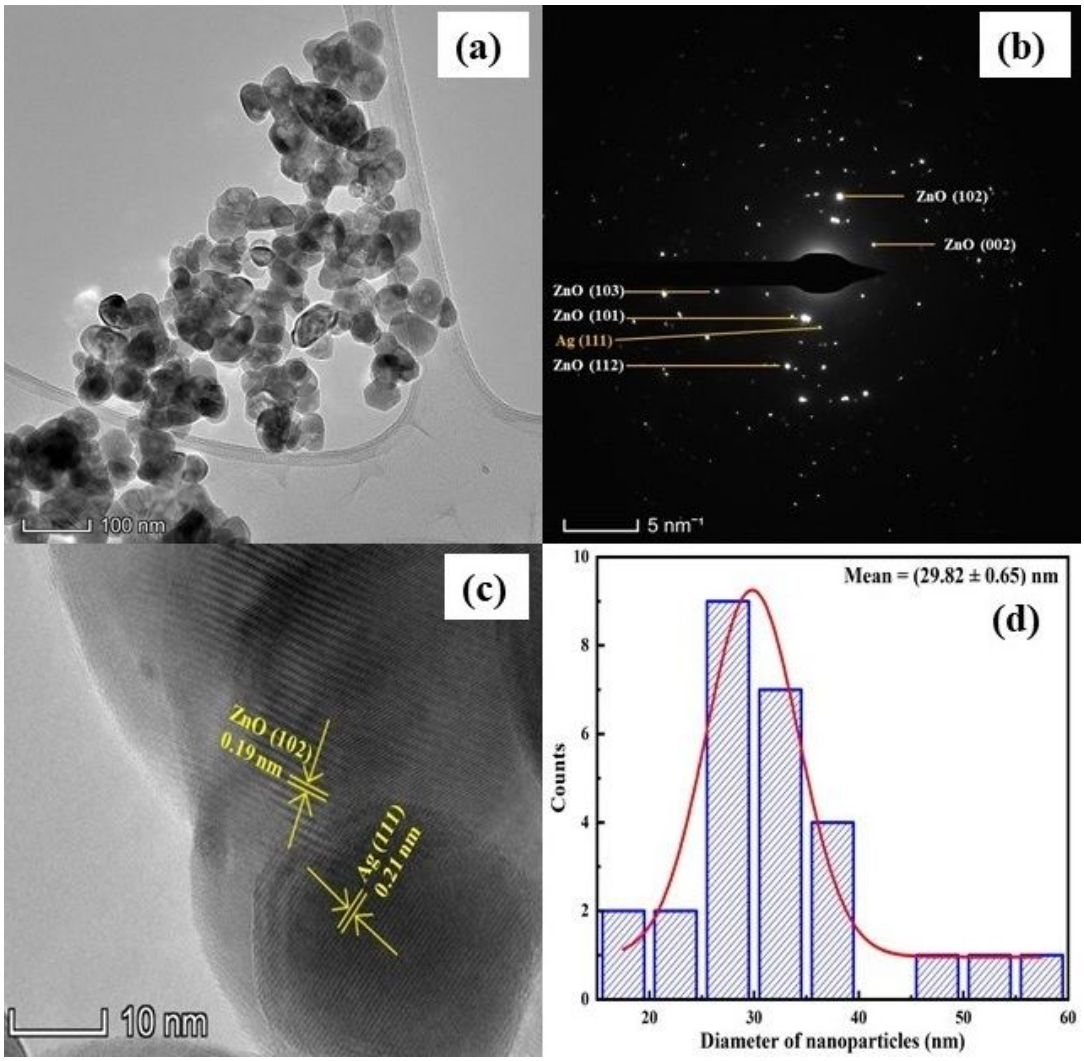

Figure 5

(a) TEM image AgZ-5 NPs, (b) SAED of AgZ-5 nanoparticles, (c) HRTEM image of AgZ-5 NPs, and (d) Histogram of AgZ-5 NPs distribution.

Figure 6

EDS spectrum of AgZ-5 nanocomposites.

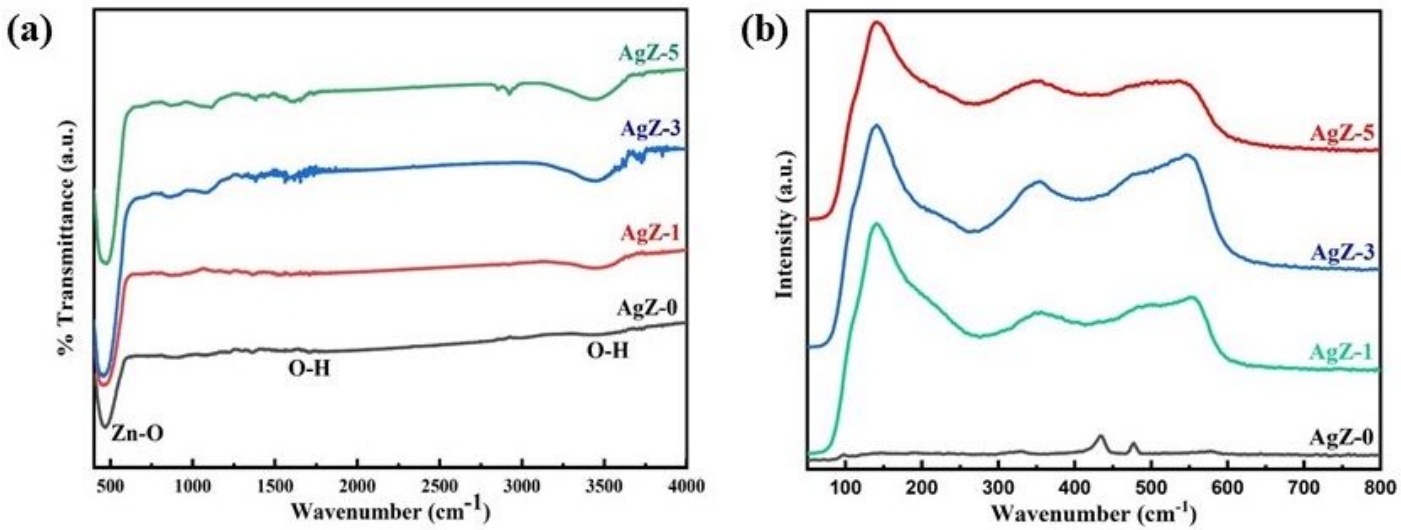

Figure 7

(a) FTIR spectra and (b) Raman spectra of all samples.

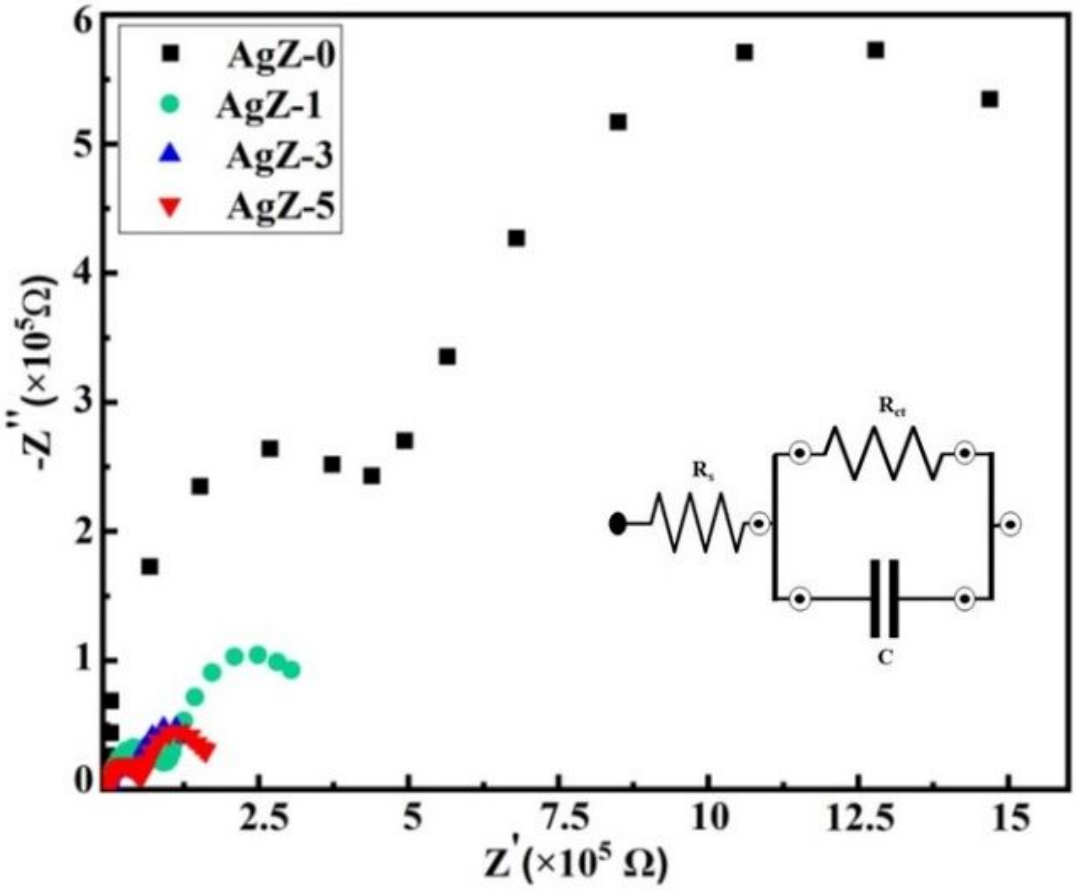

Figure 8

Nyquist plots for the Ag-doped ZnO samples.

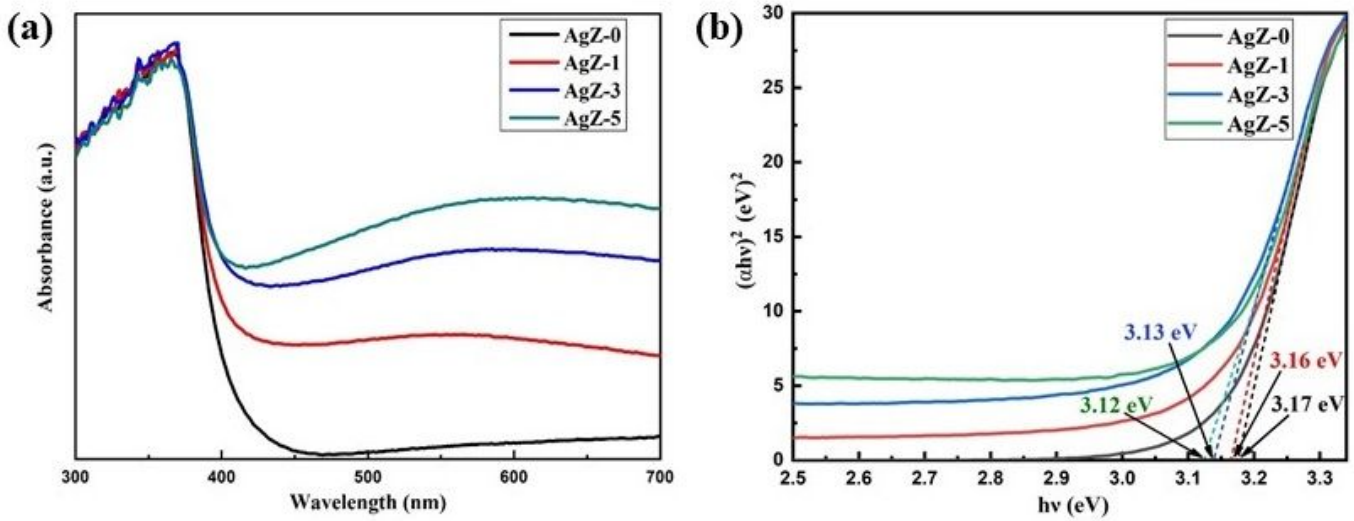

Figure 9

(a) Absorbance spectra of prepared samples and (b) Band gap calculations of prepared samples using Tauc's plot.

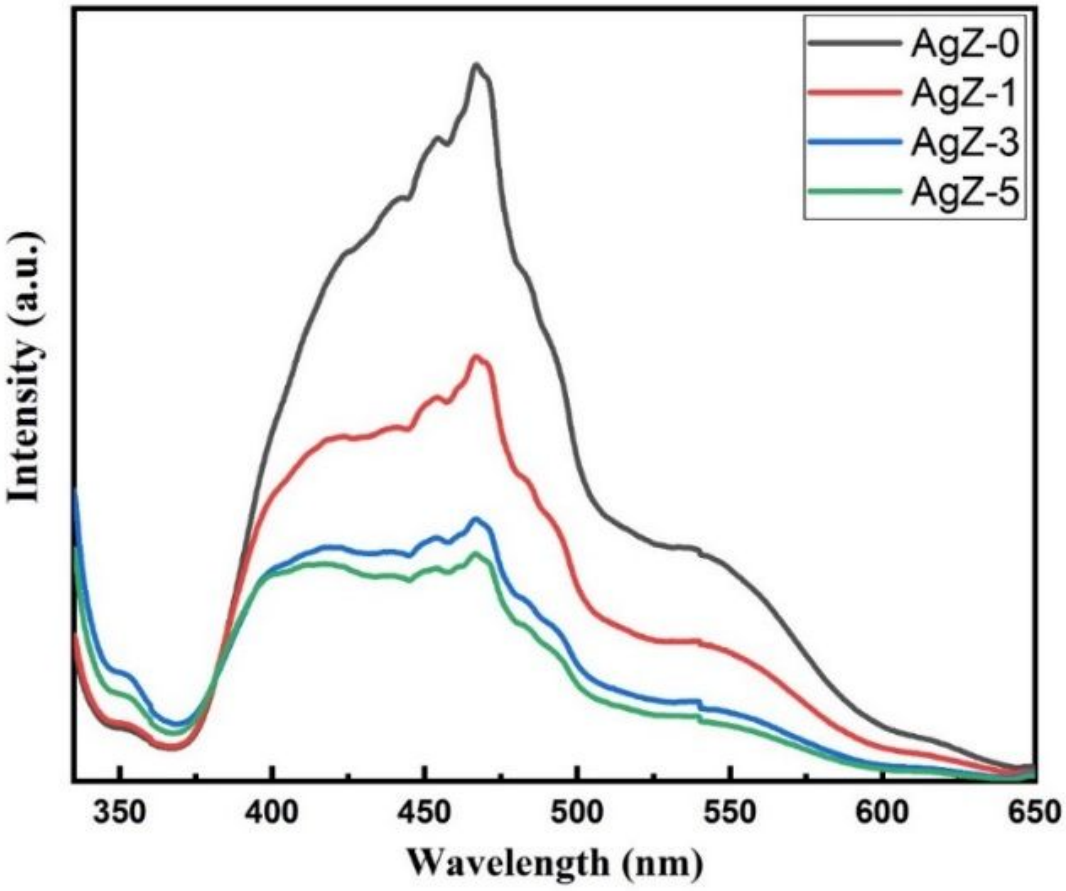

Figure 10

Photoluminescence spectra of prepared samples.

Figure 11

(a) Absorption spectra of IC dye under visible light irradiation for AgZ-5 sample, (b) Concentration changes of IC dye as the function of the illumination time, (c)The first-order kinetics of IC photocatalytic degradation, and (d) Degradation efficiency plot for IC dye.

Figure 12

(a) Mechanism for the photocatalytic degradation of IC dye using Ag/ZnO nanocomposites under visible light and (b) Study of various radical scavengers for AgZ-5 photocatalyst.